

ARTICLE

Open Access

# Malignant pleural mesothelioma co-opts BCL-X<sub>L</sub> and autophagy to escape apoptosis

Duo Xu<sup>1,2</sup>, Shun-Qing Liang<sup>1,2</sup>, Zhang Yang<sup>1,2</sup>, Haitang Yang<sup>1,2</sup>, Rémy Bruggmann<sup>1,2</sup>, Simone Oberhaensli<sup>3</sup>, Sabina Berezowska<sup>1,2</sup>, Thomas M. Marti<sup>1,2</sup>, Sean R. R. Hall<sup>1,2</sup>, Patrick Dorn<sup>1,2</sup>, Gregor J. Kocher<sup>1,2</sup>, Ralph A. Schmid<sup>1,2</sup> and Ren-Wang Peng<sup>1,2</sup>

## Abstract

Escape from programmed cell death is a hallmark of cancer. In this study, we investigated the anti-apoptotic mechanisms and explored the therapeutic potential of BCL-2 homology domain-3 (BH3) mimetics in malignant pleural mesothelioma (MPM), a lethal thoracic malignancy with an extreme dearth of treatment options. By implementing integrated analysis of functional genomic data of MPM cells and quantitative proteomics of patients' tumors, we identified BCL-X<sub>L</sub> as an anti-apoptotic driver that is overexpressed and confers an oncogenic dependency in MPM. MPM cells harboring genetic alterations that inactivate the NF2/LATS1/2 signaling are associated with increased sensitivity to A-1155463, a BCL-X<sub>L</sub>-selective BH3 mimetic. Importantly, BCL-X<sub>L</sub> inhibition elicits protective autophagy, and concomitant blockade of BCL-X<sub>L</sub> and autophagic machinery with A-1155463 and hydroxychloroquine (HCQ), the US Food and Drug Administration (FDA)-approved autophagy inhibitor, synergistically enhances anti-MPM effects in vitro and in vivo. Together, our work delineates the molecular basis underlying resistance to apoptosis and uncovers an evasive mechanism that limits response to BH3 mimetics in MPM, suggesting a novel strategy to target this aggressive disease.

## Introduction

Malignant pleural mesothelioma (MPM) is a highly aggressive malignancy that is etiologically associated with asbestos exposure<sup>1,2</sup>. Despite the restriction of asbestos use in most countries, the incidence of MPM is still rising due in part to the long latency (around 40 years) of the interval from carcinogen exposure to tumor onset<sup>3</sup>. There are no typical clinical symptoms of mesothelioma in the early phase, and the majority of patients (80%) are diagnosed at advanced stages associated with extremely poor prognosis<sup>4</sup>. Previous studies

in MPM have revealed frequent oncogenic events enabled by genetic alterations that inactivate tumor suppressor genes, most often BRCA1 associated protein-1 (*BAP1*), neurofibromatosis type 2 (*NF2*), large tumor suppressor kinase 2 (*LATS2*), and cyclin-dependent kinase inhibitor 2A/2B (*CDKN2A/2B*), which, however, have proven difficult to be therapeutically exploited<sup>2,5,6</sup>. Further exacerbating the dilemma, platinum-based chemotherapy, the current standard of care for inoperable late-stage MPM, only marginally improves patient survival<sup>7</sup>. Hence, there is a pressing need to identify new druggable targets in MPM and develop effective therapeutic strategies for the daunting disease.

The *NF2* tumor suppressor gene encodes Merlin (Moesin-ezrin-radixin-like protein), which mediates tumor suppression and contact-dependent inhibition by repressing Hippo, mTORC1, RAS, EGFR, and FAK-Src signaling pathways<sup>8</sup>. The Hippo signaling, an evolutionarily conserved pathway that regulates organ size and

Correspondence: Ralph A. Schmid (Ralph.Schmid@insel.ch) or Ren-Wang Peng (Renwang.Peng@insel.ch)

<sup>1</sup>Division of General Thoracic Surgery, Inselspital, Bern University Hospital, Bern, Switzerland

<sup>2</sup>Department for BioMedical Research (DBMR), University of Bern, Bern, Switzerland

Full list of author information is available at the end of the article

These authors contributed equally: Duo Xu, Shun-Qing Liang, Zhang Yang  
Edited by N. Barlev

© The Author(s) 2021

 Open Access This article is licensed under a Creative Commons Attribution 4.0 International License, which permits use, sharing, adaptation, distribution and reproduction in any medium or format, as long as you give appropriate credit to the original author(s) and the source, provide a link to the Creative Commons license, and indicate if changes were made. The images or other third party material in this article are included in the article's Creative Commons license, unless indicated otherwise in a credit line to the material. If material is not included in the article's Creative Commons license and your intended use is not permitted by statutory regulation or exceeds the permitted use, you will need to obtain permission directly from the copyright holder. To view a copy of this license, visit <http://creativecommons.org/licenses/by/4.0/>.

tissue homeostasis by restricting cell growth and promoting apoptosis, is one of the best characterized Merlin/NF2-regulated pathways<sup>9</sup>. Besides the mutation in *NF2*, other components of the Hippo pathway, e.g., large tumor suppressor kinase 1/2 (*LATS1/2*), are also frequently inactivated in MPM patients<sup>6</sup>. Dysregulation of the Hippo pathway constitutively activates Yes-associated protein (YAP), a transcription regulator that promotes the transcription of genes involved in cell proliferation and anti-apoptosis by interaction with TEA/ATTS domain (TEAD) transcription factors<sup>10</sup>.

Resistance to apoptosis, a critical barrier of tumor development, is one of the most prominent hallmarks of cancer<sup>11</sup>. Overexpression of pro-survival B-cell lymphoma 2 (BCL-2) family members (BCL-2, BCL-X<sub>L</sub>, MCL-1, BCL-W, BCL-B, and BFL-1) is a key apoptosis evasion mechanism that promotes tumor growth by keeping pro-apoptosis effectors (BAX/BAK) in check<sup>11</sup>. By contrast, the BCL-2 homology domain-3 (BH3)-only proteins (BAD, BIM, BID, NOXA, PUMA, BIK, BMF, and HRK) induce apoptosis by neutralizing the pro-survival BCL-2 proteins<sup>12</sup>. As such, targeting anti-apoptotic regulators with BH3 mimetics represents an attractive strategy for cancer therapy<sup>13</sup>. Several BH3 mimetics, e.g., the BCL-2/BCL-X<sub>L</sub>/BCL-W inhibitor ABT-263 (navitoclax), BCL-2-selective inhibitor venetoclax (ABT-199), and BCL-X<sub>L</sub>-selective inhibitor A-1155463, have showed promising clinical activity<sup>14</sup>. In particular, venetoclax has been approved by the US Food and Drug Administration (FDA) for the treatment of chronic lymphocytic leukemia (CLL) with a 17p-deletion or TP53 mutation<sup>15</sup>. We and others have reported that MPM cells can acquire anti-apoptotic adaptation as a protective mechanism to evade oncogenic stress and anticancer therapy<sup>16–18</sup>. In this study, we systematically analyzed the cell survival dependency on anti-apoptotic BCL-2 proteins and explored the potential of specific BH3 mimetics as anti-MPM therapy.

## Materials and methods

### Cell culture and reagents

Human normal mesothelial cells (LP-9) was a gift from Robert Kratzke (Masonic Cancer Center, University of Minnesota, USA)<sup>19</sup> and cultured in Medium 199 (Cat. #M7528; Sigma-Aldrich) supplemented with 15% fetal bovine serum (Cat. #10270-106; Life Technologies), 1% penicillin/streptomycin solution (Cat. #P0781, Sigma-Aldrich), 10 ng/ml of epidermal growth factor (Cat. #E5036, Sigma-Aldrich), and 0.4 µg/ml hydrocortisone (Cat. #07904, STEMCELL TECHNOLOGIES) at 37 °C with 95% air/5% CO<sub>2</sub>. Human normal lung fibroblasts (hFb16Lu; CCD-16Lu) and human MPM cell lines (MESO-1, MESO-4, JL-1, H2452, MSTO-211H, and H2052) were previously described<sup>18,20</sup>. All cells were authenticated by short tandem repeat (STR) profiling and

regularly tested free of mycoplasma (Microsynth). A-1155463 (Cat. #CS-5398), hydroxychloroquine (Cat. #CS-8017), Venetoclax (Cat. #S8048), and ABT-263 (Cat. #S1001) were obtained from ChemScene and SelleckChem, respectively. Bafilomycin A1 was provided by K. Krempaska (Department for Biomedical Research, University of Bern, Switzerland).

### Cell viability and clonogenic survival assay

Cell viability was measured by acid phosphatase (APH) assay as described<sup>18,20</sup>. Each data point was generated in triplicate from three independent experiments ( $n = 3$ ). IC<sub>50</sub> values were determined based on the best-fit curve generated in GraphPad Prism [log (inhibitor) vs. normalized response]. Combination Index (CI) was calculated by ComboSyn software<sup>21</sup>. CI < 1.0, synergism; CI = 1.0, additive effects, CI > 1.0, antagonism. Clonogenic assay was done as described<sup>18,20</sup>. Briefly, cells seeded in 6-well plates (1000–2000 cells/well) were treated for 96 h and cultured in the absence of drugs for 10–12 days depending on growth rate. The resulting colonies were stained with crystal violet (0.5% dissolved in 25% methanol).

### Immunoblotting and immunohistochemistry

Cell lysates were prepared and immunoblot analysis was performed as described<sup>18,22</sup>. In brief, protein lysates were resolved by SDS-PAGE (Cat. #4561033; Bio-Rad Laboratories) and transferred onto nitrocellulose membranes (Cat. #170-4158; Bio-Rad). After incubation with blocking buffer (Cat. #927-4000; Li-COR Biosciences) for 1 h at room temperature, membranes were incubated with primary antibodies (BCL-X<sub>L</sub>: 1:1000, #2764; Cleaved Caspase-7: 1:1000, #9491; LC3B: 1:500, #12741; Beclin-1: 1:1000, #3495; p62: 1:500, #5114; ATG5: 1:1000, #12994; Cell Signaling Technology) overnight at 4 °C. IRDye 680LT-conjugated goat anti-mouse IgG (Cat. #926-68020) and IRDye 800CW-conjugated goat anti-rabbit IgG (Cat. #926-32211) from Li-COR Biosciences were used at 1:10000 dilutions. Signals of membrane-bound secondary antibodies were visualized by the Odyssey Infrared Imaging System (Li-COR Biosciences), followed by quantification using Image J<sup>23</sup>.

Immunohistochemical study were performed as described<sup>24</sup>. In brief, surgically removed xenograft tumors (two tumors/group) were formalin-fixed, paraffin-embedded (FFPE), and stained with hematoxylin and eosin (H&E) using standard protocols. FFPE tissue blocks were sectioned at 4 µm, deparaffinized, rehydrated, and subsequently stained with appropriate antibodies (LC3B: 1:4000, #3868, Cell Signaling Technology; p62: 1:8000, #WH0008878M1, Sigma; Cleaved Caspase-3: 1:200; #9664, Cell Signaling Technology) using the automated system BOND RX (Leica Biosystems)<sup>24</sup>. Visualization was

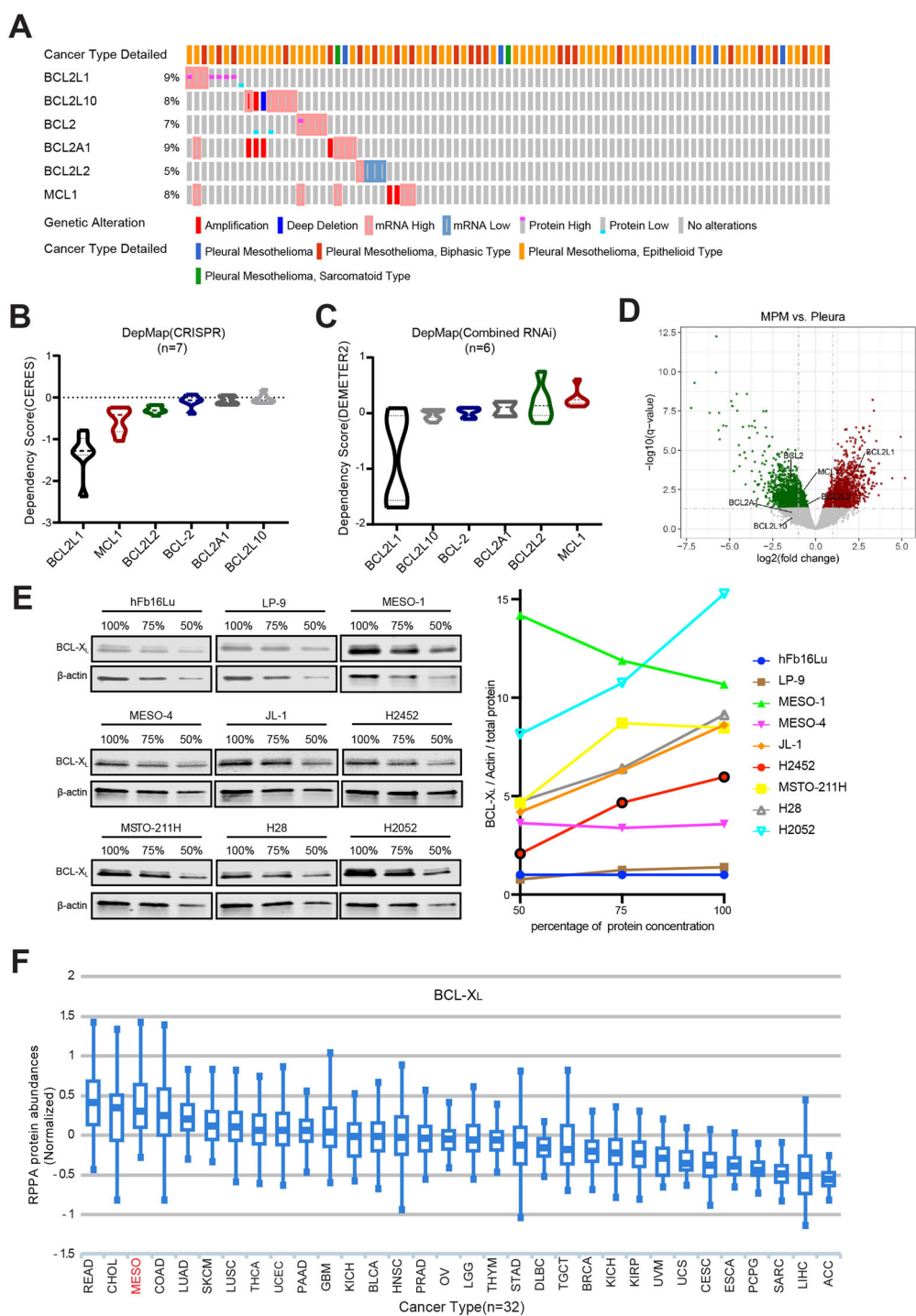


**Fig. 1** (See legend on next page.)

performed using the Bond Polymer Refine Detection kit (Leica Biosystems) as instructed by the manufacturer. Images were acquired using PANNORAMIC® whole slide scanners and processed using Case Viewer (3DHISTECH Ltd.). The staining intensities of the whole slide (two tumors/group) were quantified by QuPath software<sup>25</sup>.

#### Apoptosis assay

MPM cells were treated as specified in the figure legends. After treatment, cells in the supernatant and adherent to plates were collected, washed with PBS, and pooled before suspended in 400 µl binding buffer and stained with the Annexin V Apoptosis Detection Kit-FITC (Cat. #88-8005;

(see figure on previous page)

**Fig. 1 BCL-X<sub>L</sub> is overexpressed and confers a survival dependency in MPM.** **A** Genetic alterations and mRNA/protein expression of pro-survival Bcl-2 family genes in the TCGA cohort of MPM patients ( $n = 87$ ). Data were downloaded from the cBio Cancer Genomics Portal (CBioPortal). **B, C** The dependency profile of pro-survival BCL-2 family genes (*BCL2L1*, *BCL2L10*, *BCL2*, *BCL2A1*, *BCL2L2*, and *MCL1*) in MPM cell lines based on genome-wide CRISPR (NCIH28, NCIH2452, MPP89, NCIH2052, ISTMES2, MERO14, and MSTO-211H) or RNAi interference (MPP89, ACCMESO-1, NCI-H28, NCIH2452, NCI-H2052, and JL-1) screens. Data were downloaded from The Cancer Dependency Map Project (DepMap) datasets: CRISPR (Avana) Public 19Q3 and Combined RNAi (Broad, Novartis, Marcotte). **D** Volcano plot of transcriptomic comparison between patients' MPM samples ( $n = 40$ ) versus normal pleural tissues ( $n = 5$ ) (GSE2549). Genes significantly downregulated (adjusted  $p$  value  $<0.05$ ) are shown in green and genes significantly upregulated in red. The differentially expressed pro-survival Bcl-2 family genes are highlighted. **E** Immunoblots of BCL-X<sub>L</sub> in human normal fibroblasts (hFB16Lu), normal mesothelial cells (LP-9), and MPM cells. Proteins lysates prepared from the cells were subjected to serial dilutions (100, 75, and 50%) for immunoblot analysis (left). Densitometric analysis of the immunoblot (right) showed fold change of BCL-X<sub>L</sub> signal normalized against Actin and the total protein, with the value of hFB16Lu cells set to 1. **F** BCL-X<sub>L</sub> protein level in TCGA pan-cancer cohort ( $n = 32$ ). The expression profile was obtained from The Cancer Proteome Atlas (TCPA). READ rectum adenocarcinoma, CHOL cholangiocarcinoma, MESO mesothelioma, COAD colon adenocarcinoma, LUAD lung adenocarcinoma, SKCM skin cutaneous melanoma, LUSC lung squamous cell carcinoma, THCA thyroid carcinoma, UCEC uterine corpus endometrial carcinoma, PAAD pancreatic adenocarcinoma, GBM glioblastoma multiforme, KICH kidney chromophobe, BLCA bladder urothelial carcinoma, HNSC head and neck squamous cell carcinoma, PRAD prostate adenocarcinoma, OV ovarian serous cystadenocarcinoma, LGG brain lower grade glioma, THYM thymoma, STAD stomach adenocarcinoma, DLBC lymphoid neoplasm diffuse large B-cell lymphoma, TGCT testicular germ cell tumors, BRCA breast invasive carcinoma, KICH kidney chromophobe, KIRP kidney renal papillary cell carcinoma, UVM uveal melanoma, UCS uterine carcinosarcoma, CESC cervical squamous cell carcinoma and endocervical adenocarcinoma, ESCA esophageal carcinoma, PCPG pheochromocytoma and paraganglioma, SARC sarcoma, LIHC liver hepatocellular carcinoma, ACC adrenocortical carcinoma.

Thermo Fisher Scientific) according to the manufacturer's instructions. Flow cytometry analysis was performed on a BD Biosciences LSRII flow cytometer.

#### Autophagic flux assay

The mCherry-eGFP-LC3B lentivirus was kindly provided by Mario P. Tschan (Institute of Pathology, University of Bern, Switzerland). Briefly, lentivirus was transduced into cell lines followed by selection with puromycin (1 µg/ml) for 3 days and various treatments. Cells were then trypsinized and resuspended for flow cytometry analysis of GFP and mCherry fluorescence using a BD Biosciences LSRII flow cytometer. Data were analyzed by FlowJo software and gates for populations with low/intermediate/high mCherry/GFP ratio were set according to previous studies<sup>26,27</sup>.

#### Small interfering RNA (siRNA) knockdown

Knockdown of *BCL2L1* and *ATG5* was achieved by specific duplex siRNAs (*BCL2L1* siRNA, 15 nM; *ATG5* siRNA, 30 nM) purchased from Origene Technologies (Cat. #SR319459 and SR322789). Transfection of siRNAs was performed with Lipofectamine 2000 (Cat. #116628027, Invitrogen) according to the manufacturer's instructions.

#### Animal experiments

Mouse experiments were conducted in accordance with Institutional Animal Care and Ethical Committee-approved animal guidelines and protocols. Experiments were performed in 8-week-old male NSG (NOD-*scid* *IL2Ry*<sup>null</sup>) mice, with sample size not predetermined by statistical method but rather based on preliminary experiments. Group allocation was performed in a randomized

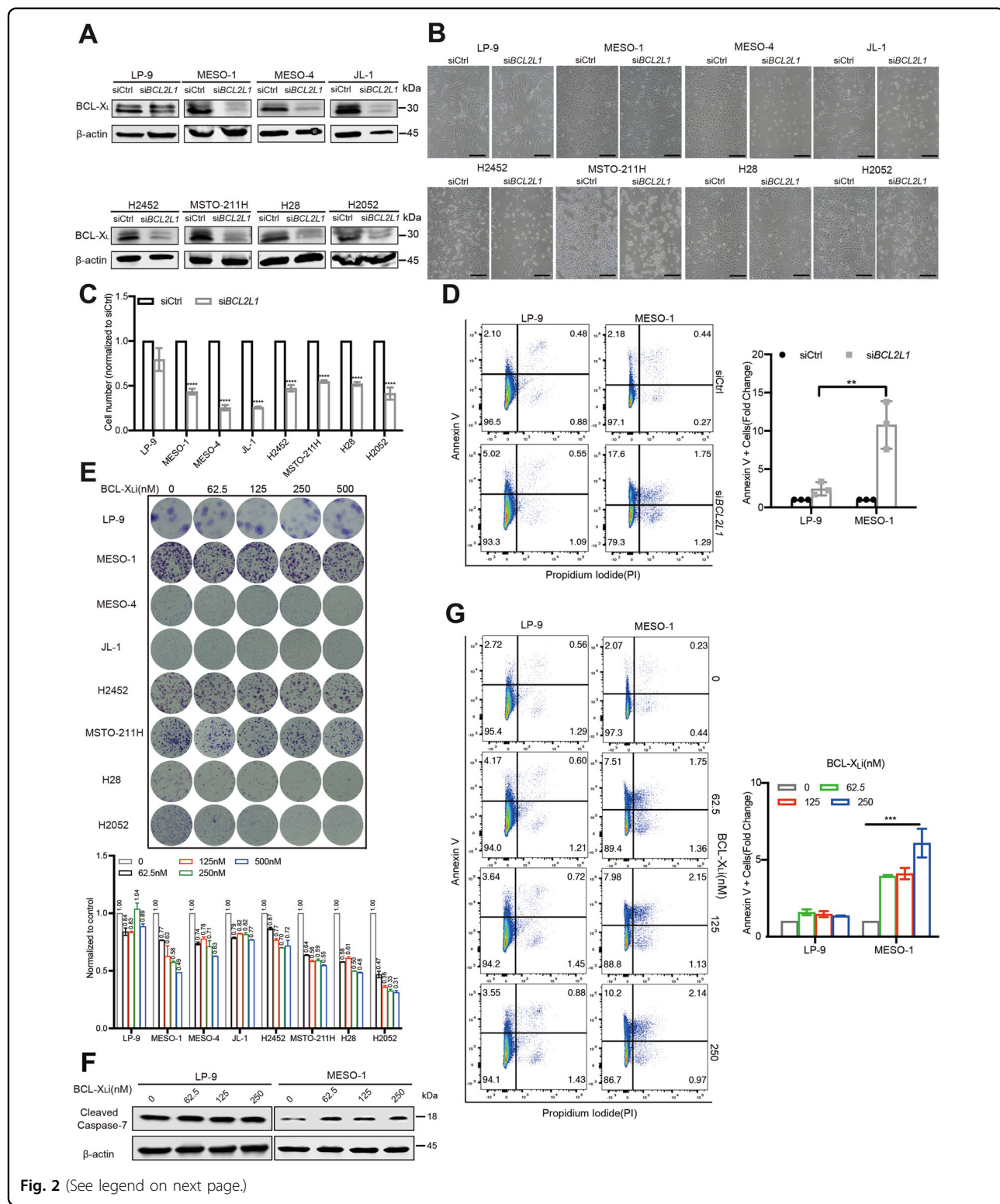
but not blinded manner. Suspensions of MESO-1 cells mixed 1:1 with Matrigel (Cat. #356231; Corning) were subcutaneously inoculated in the flanks ( $1 \times 10^6$  cells/injection). One month after injection, mice were randomly assigned to treatment groups ( $n = 5$ ): (1) control; (2) A-1155463 (5 mg/kg, i.p., once daily); (3) HCQ (50 mg/kg, i.p., once daily); (4) combination of A-1155463 and HCQ in the abovementioned doses (Tumor size was measured by digital caliper every two to three days. Tumor volume was calculated as follows: (length x width x width)/2. Mice were sacrificed at the end of 23-day treatment.

#### Public databases (TCGA, TCPA, CBioPortal, DepMap, GEO, GSDC, and COSMIC)

Interrogation of publicly available dataset was performed as we have described<sup>28</sup>. Specifically, transcriptome profiling and reverse-phase protein array data of mesothelioma patients were obtained from the Cancer Genome Atlas (TCGA), the Cancer Proteome Atlas (TCPA), and the cBio Cancer Genomics Portal (CBioPortal)<sup>29,30</sup>. The catalog of gene essentiality across MPM cell lines is obtained from the Cancer Dependency Map Project (DepMap)<sup>31</sup>. Transcriptomic data of MPM samples (GSE2549) was downloaded from the Gene Expression Omnibus(GEO)<sup>32</sup>. Genomics of Drug Sensitivity in Cancer (GDSC) and Catalog of Somatic Mutations in Cancer (COSMIC) was used to extract transcriptomic data and mutation status of MPM cell lines<sup>33,34</sup>.

#### Statistical analysis

Statistical analyses were performed using GraphPad Prism 8 (GraphPad Software, Inc.). All samples that met proper experimental conditions were included in the analysis. Data represent biological replicates ( $n$ ) and are

**Fig. 2** (See legend on next page.)

depicted as mean values  $\pm$  s.d. or mean values  $\pm$  SEM as indicated in the figure legends. Comparison of mean values was conducted with unpaired, two-tailed Student's

*t*-test, one-way or two-way ANOVA as indicated in the figure legends.  $P < 0.05$  were considered statistically significant.

(see figure on previous page)

**Fig. 2 Genetic and pharmacological inhibition of BCL-X<sub>L</sub> preferentially impairs MPM cell proliferation.** **A-C** Immunoblots (**A**) and micrographic images (**B**) of LP-9 and MPM cells with siRNA-based *BCL2L1* knockdown. Viable cells were counted 48 h post-transfection by trypan blue dye exclusion (**C**). Data were presented as mean ± s.d. ( $n = 3$ ). \*\*\* $p < 0.0001$  by two-way ANOVA with Tukey's multiple comparisons test. Scale bar: 50  $\mu$ m. **D** Flow cytometry-based apoptotic assay of LP-9 and MESO-1 cells 48 h post-transfection with siRNAs. Shown on the right is fold change in apoptotic cells (Annexin V-positive) induced by *BCL2L1* knockdown (si*BCL2L1*) compared with control siRNA (siCtrl), with the value of the control treatment set as 1. Data were presented as mean ± s.d. ( $n = 3$ ), with a representative plot shown in the left. \*\* $p < 0.01$  by two-way ANOVA with Tukey's multiple comparisons test. **E** Clonogenic assay of LP-9 and MPM cells treated with A-1155463 for 96 h and subsequently cultured in the absence of the drug for additional 12 days. Quantification is shown underneath, with data presented as mean ± s.d. ( $n = 2$ ). **F** Immunoblots of LP-9 and MESO-1 cells treated with A-1155463 for 24 h. **G** Flow cytometry-based apoptotic assay of LP-9 and MESO-1 cells after treatment with A-1155463 for 48 h. Shown on the right is fold change in apoptotic cells (Annexin V-positive) induced by treatment with A-1155463 treatment (BCL-X<sub>L</sub>i) compared with vehicle control (0 nM), with the value of the control treatment set as 1. Data were presented as mean ± s.d. ( $n = 3$ ), with a representative plot shown in the left. \*\*\* $p < 0.001$  by two-way ANOVA with Tukey's multiple comparisons test.

## Results

### BCL-X<sub>L</sub> is deregulated and confers a survival dependency in MPM

In the attempt to explore the potential of BH3 mimetics as anti-MPM therapy, we investigated genetic status, transcriptional expression, and dependency profile of the pro-survival BCL-2 gene family (*BCL2L1*, *BCL2L10*, *BCL2*, *BCL2A1*, *BCL2L2*, and *MCL1*) in MPM by interrogating TCGA dataset and functional genomics that determines genetic dependencies in cancers (DepMap; <https://depmap.org/portal/>). The integrated molecular characterization revealed that, of the anti-apoptotic genes, *BCL2L1* (encoding BCL-X<sub>L</sub>) is altered in a subset of MPM patients ( $n = 87$ ), by means of gene amplification and mRNA overexpression (Fig. 1A) and MPM cells show the greatest dependency on *BCL2L1* for survival (Fig. 1B, C). Consistently, *BCL2L1* expression is significantly upregulated in patients' MPM compared with that in normal pleural tissues (Fig. 1D). Our immunoblot analysis revealed upregulated expression of BCL-X<sub>L</sub> in human MPM cell lines compared with normal lung fibroblasts (hFb16Lu) and mesothelial LP-9 cells (Supplementary Fig. 1). Notably, a remarkably greater increase in BCL-X<sub>L</sub> was observed in MPM cells compared with normal controls when BCL-X<sub>L</sub> signal was normalized against Actin (loading control) and the total protein (Fig. 1E). Further supporting these observations, examination of TCPA dataset, which provides quantitative proteomics of patient-derived pan-cancers ( $n = 32$ ), revealed that MPM had the third highest level of BCL-X<sub>L</sub> (Fig. 1F). These results indicate that anti-apoptotic BCL-X<sub>L</sub> is deregulated in MPM at genetic, transcriptional, and translational levels.

Next, we addressed whether *BCL2L1* represents a genetic vulnerability in MPM. *BCL2L1* knockdown by siRNAs caused significantly greater proliferative inhibition and apoptotic cell death in MPM cells (MESO-1, MESO-4, JL-1, H2452, MSTO-211H, H28, and H2052) than in LP-9 cells (Fig. 2A–D). Consistent with the genetic results, A-1155463, a potent and highly selective

BCL-X<sub>L</sub> inhibitor<sup>14</sup>, preferentially impaired MPM cells, resulting in significantly greater growth inhibition in MPM cells than in LP-9 cells (Fig. 2E). Importantly, A-1155463 induced cleavage of caspase-7 (Fig. 2F) and a dose-dependent increase of apoptotic cells in MESO-1, as manifested by flow cytometry-based apoptotic analysis, which showed that treatment with 62.5, 125, and 250 nm A-1155463 resulted in 4-, 4.4-, and 5.4-fold increases in apoptotic cells (Annexin V-positive) compared with vehicle treatment (Fig. 2G). In contrast, A-1155463 treatment barely increased apoptosis compared with vehicle control in LP-9 cells (Fig. 2F, G). Importantly, the selective BCL-2 inhibitor Venetoclax failed to distinguish malignant from normal mesothelial cells, leading to almost equal effects on MPM and LP-9 cells (Supplementary Fig. 2A). Taken together, these results reveal that BCL-X<sub>L</sub> is highly deregulated and confers an oncogenic dependency in MPM.

### NF2/LAST1/2 mutations are associated with increased sensitivity to BCL-X<sub>L</sub> inhibition in MPM

Next, we sought to identify potential biomarkers associated with MPM response to BCL-X<sub>L</sub> inhibition in MPM. As expected, the BCL-X<sub>L</sub> protein level was positively correlated with the sensitivity to A-1155463 [negatively with the IC<sub>50</sub> (50% inhibitory concentration)] in MPM cells (Fig. 3A, B).

It has been shown that cancer cells express high levels of pro-apoptotic proteins that, however, are constrained via heterodimerization by anti-apoptotic effectors during tumorigenesis<sup>11,35</sup>. As a result, cancer cells can be considered to be ready to undergo apoptosis or “primed for apoptosis”, highlighting the potential of BH3 mimetics in the clinic<sup>36</sup>. To explore a possible link of *BCL2L1* with pro-apoptotic proteins in MPM, we examined a cohort of MPM patients ( $n = 87$ ) in TCGA, which revealed that *BCL2L1* mRNA level was positively correlated with that of several pro-apoptotic genes, e.g., *BAX*, *BBC3*, *BIK*, and *BAK1* (Fig. 3C). Consistent with this observation, MPM cells that overexpress BCL-X<sub>L</sub> also have higher protein

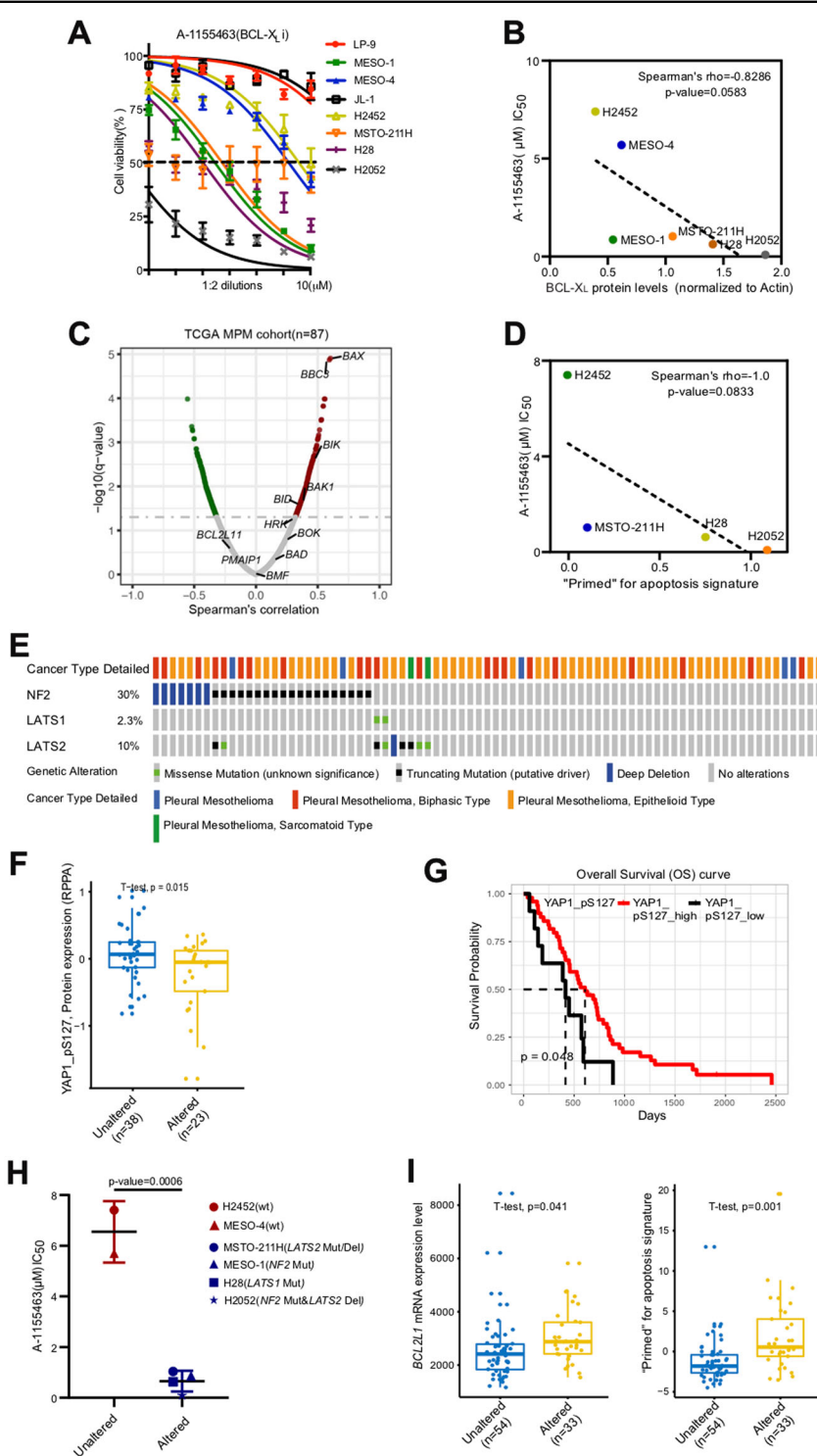


**Fig. 3** (See legend on next page.)

levels of BAX (Supplementary Fig. 2B), suggesting that *BCL2L1*-positive MPM tumors are “primed” to apoptosis induction. By using a previously defined “primed for apoptosis” gene signature, determined by transcriptional

expression of the pro-apoptotic genes (*BAK1*, *BAX*, *BBC3*, *BID*, *BIK*, *BOK*, and *HRK*)<sup>37</sup>, we curated the “primed for apoptosis” score of H2452, MSTO-211H, H28, and H2052 cells, chosen for the availability of their transcriptomic

(see figure on previous page)

**Fig. 3 NF2/LATS1/2 mutations are associated with increased sensitivity to BCL-X<sub>L</sub> inhibition in MPM cells.** **A** Cell viability assay of LP-9 and a panel of MPM cell lines treated with A-1155463 for 96 h. Data were presented as mean  $\pm$  s.d. ( $n = 3$ ). **B** Correlation analysis of BCL-X<sub>L</sub> protein levels and the 50% inhibitory concentration (IC<sub>50</sub>) values of A-1155463 in MPM cell lines. **C** Volcano plot of Spearman's rank correlation coefficient between gene expression of *BCL2L1* and that of pro-apoptotic genes in patients' MPM samples ( $n = 87$ ). Data were downloaded from TCGA and subsequently analyzed by R software (Cor.test function). **D** Correlation analysis of "primed" for apoptosis signature (based on the sum of gene expression of *BAK1*, *BAX*, *BBC3*, *BID*, *BIK*, *BOK*, and *HRK*) and the IC<sub>50</sub> of A-1155463 in MPM cell lines. Transcriptomic data of the indicated MPM cell lines were extracted from Catalog of Somatic Mutations in Cancer (COSMIC). **E** Genetic status of *NF2/LATS1/2* in TCGA cohort of MPM patients ( $n = 87$ ). Data were downloaded from cBioPortal. **F** Genetic alterations in *NF2/LATS1/2* are associated with decreased protein level of YAP1\_pS127. MPM patients ( $n = 61$ ) in a TCGA cohort were stratified according to *NF2/LATS1/2* genetic status (altered or unaltered), with  $p$  value calculated by unpaired, two-tailed Student's *t*-test. **G** Kaplan–Meier curves showing overall survival (OS) of a TCGA cohort of MPM patients ( $n = 61$ ) stratified by protein level of YAP1\_pS127 (high versus low). The  $p$  value is calculated by the log-rank test using R (version 3.4.3). **H** *NF2/LATS1/2*-mutant MPM cells showed increased sensitivity to A-1155463 (IC<sub>50</sub>). MPM cells were grouped according to genetic status of *NF2/LATS1/2*, with  $p$  value calculated by unpaired, two-tailed Student's *t*-test. WT, no alterations in *NF2/LATS1/2*. **I** Genetic alterations in *NF2/LATS1/2* are associated with increased *BCL2L1* mRNA levels and with a higher gene signature "primed" for apoptosis. MPM patients of a TCGA cohort ( $n = 87$ ) were grouped according to *NF2/LATS1/2* genetic status in the tumors (altered or unaltered).  $p$  value was calculated by unpaired, two-tailed Student's *t*-test.

data in the Catalog of Somatic Mutations in Cancer (COSMIC). Our analysis revealed that MPM cells with higher scores of the apoptosis gene signature were more sensitive (lower IC<sub>50</sub> values) to A-1155463 (Fig. 3D), supporting the notion that expression of the pro-apoptotic genes predicts BCL-X<sub>L</sub> inhibitor sensitivity.

Finally, we explored if recurrent genetic alterations in MPM are associated with sensitivity to BCL-X<sub>L</sub> inhibition. *NF2/LATS1/2* loss of function (deletion, truncation, and mutation) is frequent (38%) in MPM (Fig. 3E), which downregulates YAP phosphorylation (YAP1\_pS127) and increases the activity of YAP oncprotein (Fig. 3F). Consistent with this observation, MPM patients with low levels of YAP1\_pS127 (increased YAP activity) were associated with dismal prognosis (Fig. 3G) and MPM cells harboring *NF2/LATS1/2* mutations/deletions exhibited increased sensitivity to A-1155463 (Fig. 3H). Supporting this finding, examining the TCGA cohort of MPM patients ( $n = 87$ ) showed that *NF2/LATS1/2*-altered tumors were characterized by an increased *BCL2L1* expression and "primed for apoptosis" score (Fig. 3I).

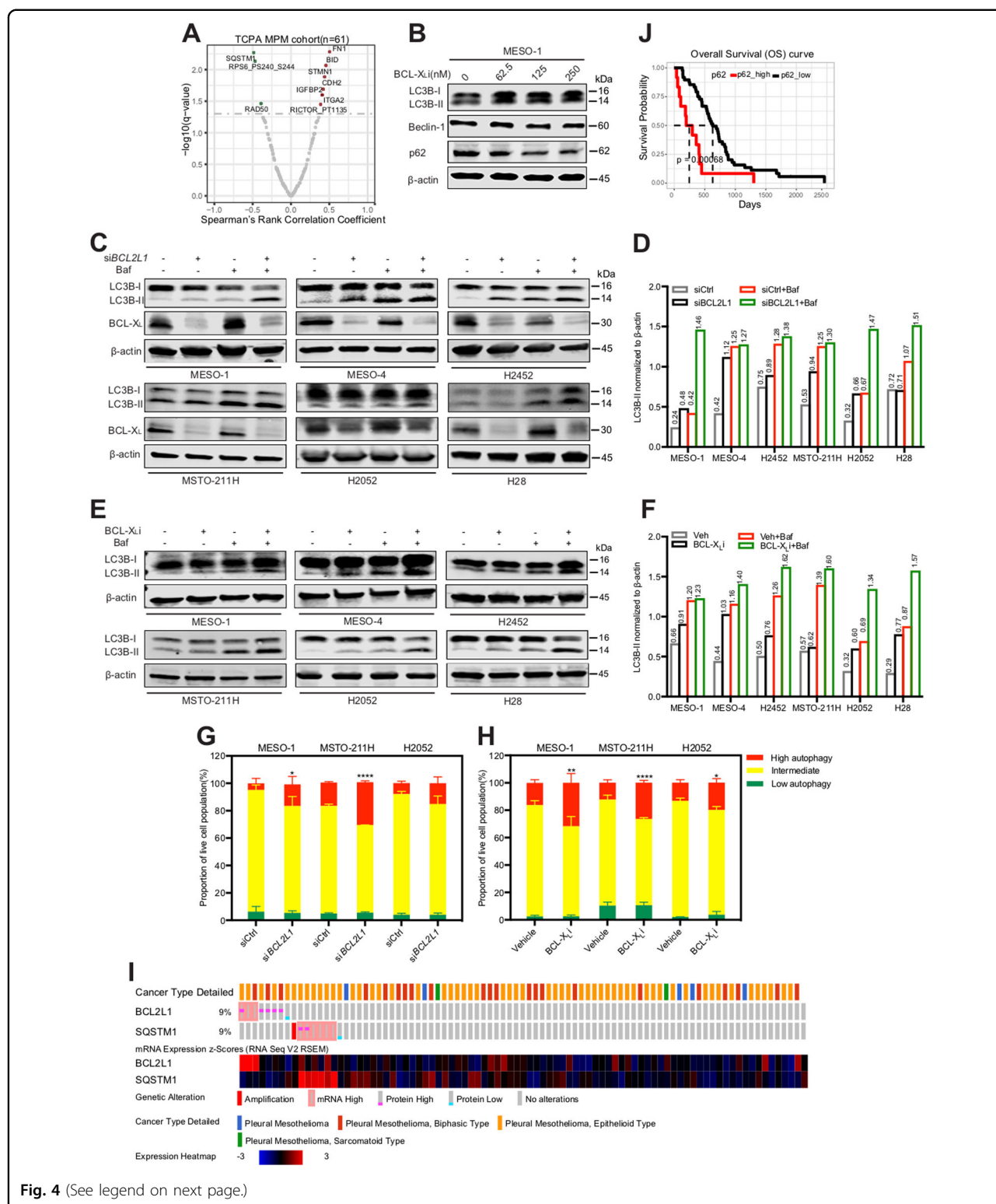
Thus, BCL-X<sub>L</sub> protein expression, "primed for apoptosis" gene signature and genetic alterations in *NF2/LATS1/2* may serve as biomarkers to stratify MPM subsets that likely benefit from BCL-X<sub>L</sub> targeted therapy.

#### BCL-X<sub>L</sub> inhibition elicits protective autophagy in MPM cells

Our observations that MPM cells show heterogeneous responses to BCL-X<sub>L</sub> inhibition (Figs. 2, 3) suggest the existence of resistance mechanisms. This prompted us to explore the approaches to improve the efficacy of BCL-X<sub>L</sub>-targeted therapy. Interrogation of TCPA dataset revealed SQSTM1 (sequestosome 1; also termed p62) as the top candidate that is significantly negatively correlated with BCL-X<sub>L</sub> (Fig. 4A). p62 is a key component of autophagic machinery functioning as a cargo adapter by physical interaction with and subsequent delivery of autophagic substrates to autophagosomes for degradation<sup>38</sup>,

suggesting a possible role for autophagy to protect MPM cells from the stress elicited by BCL-X<sub>L</sub> inhibition. Supporting our hypothesis, treatment with A-1155263 acutely increased autophagic activity in MESO-1 cells, marked by decreased p62, upregulated Beclin-1, and microtubule-associated proteins 1A/1B light chain 3B (LC3B)-II (Fig. 4B), whereby the conversion of cytosolic LC3B-I to autophagosome-localized LC3B-II is proportional with initiation of autophagy and therefore serves as a reliable marker of autophagosomes<sup>38</sup>. Moreover, genetic (siRNAs) and pharmacological (A-1155463) inhibition of BCL-X<sub>L</sub> markedly increased the LC3B-II lapidated form, in particular the ratio of LC3B-II/Actin signal, compared with vehicle controls at the basal level and in the presence of Bafilomycin A1, an inhibitor of autophagosome-lysosome fusion<sup>26,38</sup>, in a panel of MPM cells (Fig. 4C–F). In sharp contrast, the same effects of BCL-X<sub>L</sub> inhibition were not observed in LP-9 cells, as A-1155463 alone showed no effect on the LC3B-II/Actin ratio (compared with vehicle control), as did concomitant treatment with A-1155463 and Bafilomycin (compared with Bafilomycin alone) (Supplementary Fig. 2C). Importantly, using the mCherry-eGFP-LC3B fluorescence reporter<sup>26,27</sup>, we showed that genetic and pharmacological inhibition of BCL-X<sub>L</sub> significantly increased the mCherry:GFP fluorescence ratio, a well-recognized measure of autophagic flux, in MPM cells stably expressing mCherry-eGFP-LC3B (Fig. 4G, H), further strengthening the notion that BCL-X<sub>L</sub> inhibition increases autophagy.

SQSTM1/p62 deregulation (e.g., mRNA upregulation or protein overexpression) occurred in a subset (9%) of MPM patients (Fig. 4I). Although implications of SQSTM1/p62 changes can be context-dependent and deserve cautious interpretations, the steady state level of p62 do reflect the autophagic status<sup>38</sup> and it is widely accepted that impaired autophagy contributes to initiation and early development of cancer<sup>38,39</sup>. Indeed, previous studies associated decreased p62 or high autophagy status

**Fig. 4** (See legend on next page.)

with better clinical outcomes in MPM and other tumors<sup>40,41</sup>. Supporting this notion, high p62 levels predicted poorer prognosis in MPM patients, opposite to the

prognostic value of BCL-X<sub>L</sub> (Fig. 4J, Supplementary Fig. S3A). Moreover, deregulation of SQSTM1/p62 and BCL2L1 appeared mutually exclusive (Fig. 4I), reiterating

(see figure on previous page)

**Fig. 4 Genetic and pharmacological inhibition of BCL-X<sub>L</sub> increases autophagic flux in MPM cells.** **A**, Volcano plot of Spearman's rank correlation coefficient between BCL-X<sub>L</sub> and other tested proteins ( $n = 217$ ). Proteomic data were downloaded from TCPA, and proteins significantly (adjusted  $p$  value (or  $q$  value)  $<0.05$ ) correlated with BCL-X<sub>L</sub> are highlighted. **B**, Immunoblots of MESO-1 treated with A-1155463 for 24 h. **C, D**, MPM cells transiently transfected with *BCL2L1*-siRNAs (siBCL2L1) were treated (48 h post-transfection) with Baflomycin (200 nM) or vehicle (DMSO) for 2 h before subjected to immunoblots to assess autophagic flux. Protein quantification is shown in **(D)**. Note the increase in LC3B-II/Actin ratio by *BCL2L1* knockdown in the absence and presence of Baflomycin. **E, F**, MPM cells pre-treated with A-1155463 (1  $\mu$ M) for 24 h were exposed to Baflomycin (200 nM) or vehicle (DMSO) for another 2 h before immunoblot analysis. Protein quantification is shown in **(F)**. Note the increase in LC3B-II/Actin ratio by A-1155463 treatment in the absence and presence of Baflomycin. **G, H**, MPM cells stably expressing mCherry-eGFP-LC3B were transfected with *BCL2L1*-siRNA (siBCL2L1) or control siRNA for 48 h **(G)**, or treated with A-1155463 (1  $\mu$ M) or vehicle for 24 h **(H)** before analyzed by flow cytometry. Data were presented as mean  $\pm$  s.d. ( $n = 3$ ). \* $p < 0.05$ , \*\* $p < 0.01$ , and \*\*\* $p < 0.0001$  by two-way ANOVA with Sidak's multiple comparisons test of control high versus experimental high (red). **I**, Genetic status and mRNA/protein expression of *BCL2L1* and *SQSTM1* in a TCGA cohort of MPM patients ( $n = 87$ ). Data were downloaded from cBioPortal. **J**, Kaplan-Meier analysis of MPM based on p62 protein level. TCGA cohort of MPM patients ( $n = 61$ ) with high- (in red) or low-p62 (in black) were stratified by optimal cutoff value of the p62 across all patients using the surv\_cutpoint function in the R "maxstat" package. The  $p$  value is calculated by the log-rank test using R (version 3.4.3).

the reciprocal nature of p62-and BCL-X<sub>L</sub>-regulated processes in MPM development. Together, these results reveal that BCL-X<sub>L</sub> inhibition elicits autophagy, which may act as a compensatory mechanism that counteracts BCL-X<sub>L</sub> targeted therapy.

#### Concomitant blockage of BCL-X<sub>L</sub> and autophagy synergistically enhances anti-MPM effects

To test this hypothesis that autophagy protects MPM cells from the cytotoxicity of BCL-X<sub>L</sub> inhibition, MPM cells were concomitantly treated with A-1155463 and the autophagy inhibitor hydroxychloroquine (HCQ) across a broad range of concentrations. While single agents suppressed cell proliferation in a dose-dependent manner, A-1155463 plus HCQ produced a strong synergy, leading to significantly enhanced antiproliferative effects and apoptotic cell death in a panel of MPM cells, including *NF2/LATS1/2*-mutant and wild-type (Fig. 5A–E) but not in human normal lung fibroblasts (Supplementary Fig. S3B). The synergy also applied when HCQ was combined with ABT-263, a pan-inhibitor against BCL-2, BCL-X<sub>L</sub>, and BCL-W (Supplementary Fig. S3C–E).

To further explore the role of autophagy in MPM response to BCL-X<sub>L</sub> inhibition, we knocked down autophagy related 5 (*ATG5*), which encodes a key effector protein (*ATG5*) involved in the initiation of pre-autophagosome formation<sup>39</sup>. Genetic depletion of *ATG5* in MPM cells significantly enhanced the antiproliferative effects of BCL-X<sub>L</sub> inhibition (Fig. 5F, G), which is in line with the results of pharmacological studies (Fig. 5A–D). Thus, BCL-X<sub>L</sub> inhibition elicits protective autophagy and combined blockage of BCL-X<sub>L</sub> and autophagy represents a promising strategy to treat MPM.

#### BCL-X<sub>L</sub> inhibition combined with hydroxychloroquine potently suppresses MPM growth in vivo

To extend the in vitro observations to in vivo, we evaluated efficacy of the combination treatment with A-1155463 and HCQ in MESO-1 xenografts. Whereas A-1155463

alone delayed tumor growth, the addition of HCQ profoundly enhanced antitumor efficacy without obvious side effects, i.e., body weight loss (Fig. 6A–D). Immunohistochemical analysis demonstrated that tumors treated with A-1155463 alone showed enhanced punctate staining of LC3B (highlighted in insets) and reduced p62 compared with the vehicle group (Fig. 6E), consistent with an increase in the autophagic flux upon BCL-X<sub>L</sub> inhibition as we showed in vitro. Importantly, the combination treatment blunted A-1155463-elicited autophagy, accompanied by increase in tumor cell apoptosis as indicated by the increase in cleaved caspase-3 in the combination group compared with single treatment (Fig. 6E). Immunoblots indicated that drug combination of A-1155463 and HCQ increased p62 and cleaved caspase-7 compared with single agents alone (Fig. 6F), further supporting the notion that combined A-1155463 and HCQ suppresses autophagy and induces apoptosis. Overall, these in vivo data validate a novel therapeutic strategy by combined inhibition of BCL-X<sub>L</sub> and autophagy to target MPM.

#### Discussion

In this study, we showed that MPM capitalizes on BCL-X<sub>L</sub> for anti-apoptosis, and that *NF2/LATS1/2*-alterations and pro-apoptotic gene expression are associated with sensitivity to BCL-X<sub>L</sub> inhibition. We further revealed that BCL-X<sub>L</sub> blockage elicited protective autophagy, such that combined treatment with BCL-X<sub>L</sub>-selective BH3 mimetic and clinically approved autophagy inhibitor yields strong and synergistic anti-MPM effects in vitro and in vivo. Our data suggest the therapeutic potential of targeting BCL-X<sub>L</sub> alone for MPM subsets, and of co-targeting autophagy for unselected MPM.

Apoptosis is regulated by pro- and anti-apoptotic BCL-2 proteins, which is invariably deregulated in cancer<sup>11,13</sup>. In response to oncogenic or stress signals, malignant cells overexpress anti-apoptotic proteins to dampen apoptosis by sequestering pro-apoptotic activators<sup>35</sup>. In this scenario, cancer cells are proposed to be “primed” for

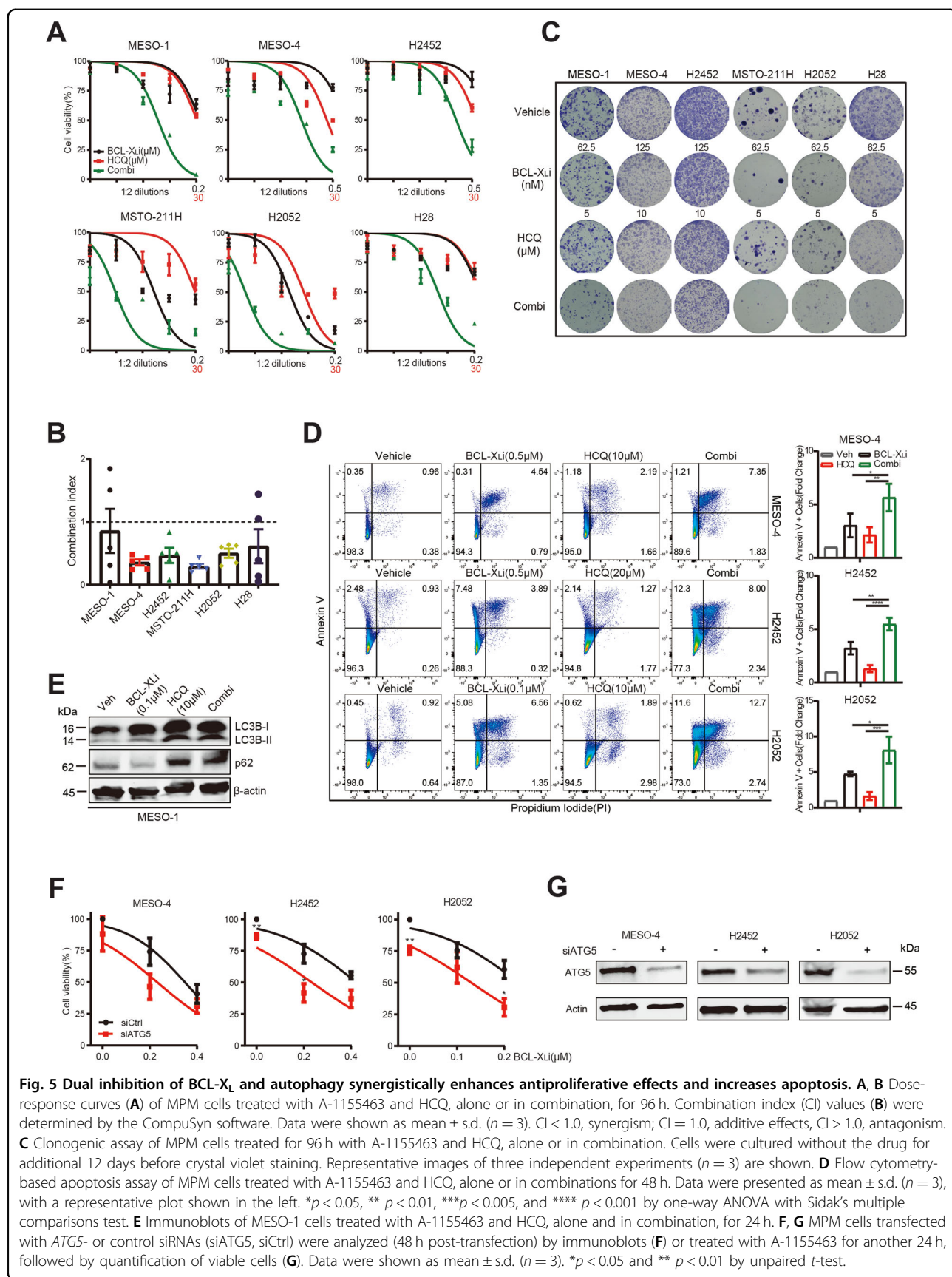


**Fig. 5 Dual inhibition of BCL-X<sub>L</sub> and autophagy synergistically enhances antiproliferative effects and increases apoptosis.** **A, B** Dose-response curves (**A**) of MPM cells treated with A-1155463 and HCQ, alone or in combination, for 96 h. Combination index (CI) values (**B**) were determined by the CompuSyn software. Data were shown as mean ± s.d. (n = 3). CI < 1.0, synergism; CI = 1.0, additive effects, CI > 1.0, antagonism. **C** Clonogenic assay of MPM cells treated for 96 h with A-1155463 and HCQ, alone or in combination. Cells were cultured without the drug for additional 12 days before crystal violet staining. Representative images of three independent experiments (n = 3) are shown. **D** Flow cytometry-based apoptosis assay of MPM cells treated with A-1155463 and HCQ, alone or in combinations for 48 h. Data were presented as mean ± s.d. (n = 3), with a representative plot shown in the left. \*p < 0.05, \*\*p < 0.01, \*\*\*p < 0.005, and \*\*\*\*p < 0.001 by one-way ANOVA with Sidak's multiple comparisons test. **E** Immunoblots of MESO-1 cells treated with A-1155463 and HCQ, alone and in combination, for 24 h. **F, G** MPM cells transfected with ATG5- or control siRNAs (siATG5, siCtrl) were analyzed (48 h post-transfection) by immunoblots (**F**) or treated with A-1155463 for another 24 h, followed by quantification of viable cells (**G**). Data were shown as mean ± s.d. (n = 3). \*p < 0.05 and \*\*p < 0.01 by unpaired t-test.

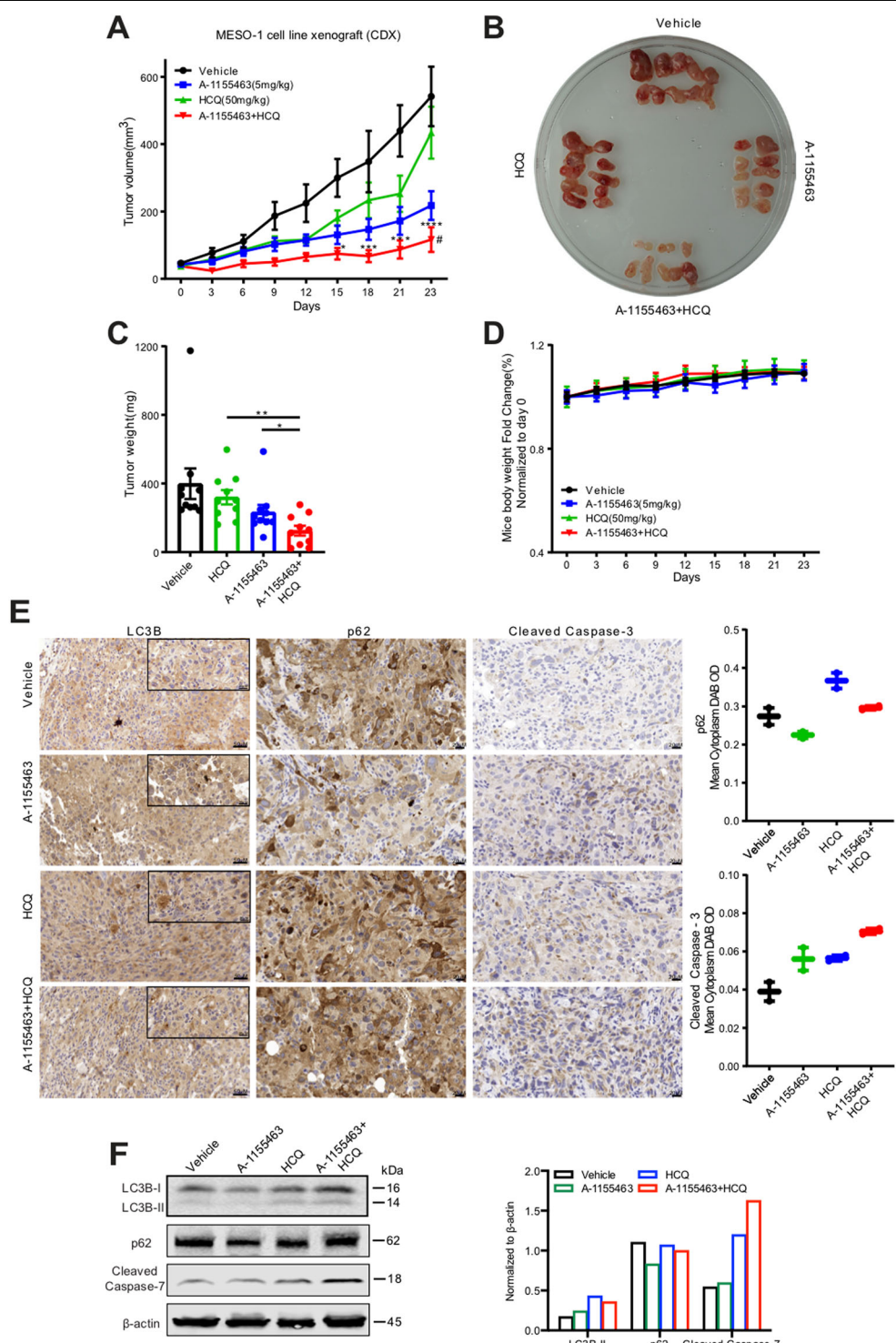


**Fig. 6** Hydroxychloroquine (HCQ) potentiates anti-MPM efficacy of A-1155463 *in vivo*. **A** Development of MESO-1 xenograft tumors treated with the indicated drugs. Data were presented as mean  $\pm$  SEM ( $n = 5$ ).  ${}^{\#}p < 0.05$ , comparison between combination (A-1155463 plus HCQ)- versus A-1155463-treated group by two-way ANOVA with Tukey's multiple comparisons test.  $*p < 0.05$ ,  $**p < 0.01$ , and  $****p < 0.0001$ , comparison between combination- versus HCQ-treated group by two-way ANOVA with Tukey's multiple comparisons test. **B, C** Tumor size (**B**) and weights (**C**) after the treatment. Data were presented as mean  $\pm$  SEM ( $n = 5$ ).  $*p < 0.05$  and  $**p < 0.01$  by unpaired *t*-test. **D** Mice body weights during the treatment. Data were presented as mean  $\pm$  SEM ( $n = 5$ ). **E** Immunohistochemical staining for LC3B, p62, and cleaved caspase-3 of MESO-1 xenograft tumors after the treatment. Quantification of p62 and cleaved Caspase-3 in the entire tissue sections were performed by QuPath. **F** Immunoblots for LC3B, p62, and cleaved caspase-7 of MESO-1 xenograft tumors after the treatment. Protein quantification is shown to the right.

apoptosis, as they accumulate sufficient amounts of the pro-apoptotic activators<sup>36</sup>, which has engendered the concept of cancer treatment by conquering or overwhelming anti-apoptotic defenses, e.g., blockage of specific or multiple pro-survival proteins with BH3 mimetics such as ABT-263 (navitoclax) and ABT-199 (venetoclax)<sup>12,42</sup>. In MPM, apoptosis suppression was reported to be promoted by defects in core-apoptosis signaling<sup>43</sup>, and the pro-apoptotic BH3 mimetic ABT-737 targeting BCL-2/BCL-X<sub>L</sub>/BCL-W<sup>44</sup> and a pan-BCL-2 inhibitor (JY-1-106) were active against MPM cells<sup>45,46</sup>. However, despite the promising clinical activity of pan-BH3 mimetic drugs, challenges still prevail due to intrinsic or/and acquired resistance and on-target platelet toxicity<sup>14,47–49</sup>, necessitating the need to dissect the survival dependency on individual BCL-2 proteins and the use of selective BH3 mimetics in clinical development. We show here that BCL-X<sub>L</sub> is a major survival dependency for MPM cells and that the BCL-X<sub>L</sub> by selective BH3 mimetic demonstrates therapeutic potential for subsets of MPM. Notably, our data are consistent with earlier observations that antagonizing BCL-X<sub>L</sub> by alternative strategies (e.g., anti-sense oligonucleotides) suppresses MPM cell survival<sup>44,50</sup> and with the finding of a very recent study<sup>51</sup> published amid the manuscript preparation of our work.

We showed for the first time that BCL-X<sub>L</sub> inhibition elicits protective autophagy that limits the efficacy of BCL-X<sub>L</sub>-selective BH3 mimetics. Autophagy and apoptosis constitute two important self-destructive processes to maintain cellular homeostasis<sup>52</sup>, and there is a complex reciprocal interplay<sup>53–55</sup>. Apoptosis activation can either increase or decrease autophagy, but the underlying mechanisms are controversial<sup>56</sup>. Recent studies have reported that inhibition of pro-survival BCL-2 proteins with BH3 mimetics could induce autophagy either by releasing Beclin-1 from the BH3-binding groove of BCL-2/BCL-X<sub>L</sub> or by BAX- and BAK1-mediated LC3B lipidation<sup>57–59</sup>. In line with this notion, we revealed that targeting autophagy with HCQ synergistically enhances the cytotoxic effect of A-1155463, suggesting that this combination may be a novel strategy for treating MPM. Notably and in further support of our findings, a recent report published amid the revision of this study showed that BCL-X<sub>L</sub> is overexpressed and is an important pro-survival protein in MPM cells<sup>60</sup>.

The lack of therapeutically exploitable mutations has significantly hampered the development of targeted therapies for MPM<sup>2,6</sup>, which, however, highlights the importance to identify oncogenic dependencies rather than specific driver mutations to combat MPM<sup>1</sup>. We have systematically assessed the pro-survival BCL-2 proteins for their contributions to anti-apoptosis in MPM cells, which, to the best of our knowledge, has remained incompletely defined. Overall, our work demonstrates the

therapeutic potential of BCL-X<sub>L</sub>-specific BH3 mimetics in MPM, alone and in combination with the FDA-approved HCQ.

#### Acknowledgements

The results published here are in part upon data generated by the TCGA Research Network: <https://www.cancer.gov/tcga>. Robert Kratzke (Masonic Cancer Center, University of Minnesota, USA) and Mario P. Tschan (Institute of Pathology, University of Bern, Switzerland) are acknowledged for kindly providing LP-9 cells and lentiviral particles expressing mCherry-eGFP-LC3B, respectively. We thank Nivia Barontini (Thoracic Surgery Laboratory, Bern University Hospital), Kristina Krempaska (Department for Biomedical Research, University of Bern, Switzerland) for technical assistance.

#### Author details

<sup>1</sup>Division of General Thoracic Surgery, Inselspital, Bern University Hospital, Bern, Switzerland. <sup>2</sup>Department for BioMedical Research (DBMR), University of Bern, Bern, Switzerland. <sup>3</sup>Interfaculty Bioinformatics Unit and Swiss Institute of Bioinformatics, University of Bern, Bern, Switzerland. <sup>4</sup>Institute of Pathology, University of Bern, Bern, Switzerland

#### Author contributions

D.X., S.-Q.L., R.A.S., and R.-W.P. contributed to design, data acquisition, analysis, and interpretation; Z.Y., H.Y., R.B., S.O., S.B., T.M.M., S.R.R.H., P.D., and G.J.K. contributed to analysis and interpretation of data; D.X. drafted the manuscript and R.-W.P. critically revised the manuscript. All authors read and agreed on the final version of the manuscript.

#### Funding

This work was funded by grants from the Swiss Cancer League/Swiss Cancer Research Foundation (#KFS-4851-08-2019; to RWP), PhD fellowships from China Scholarship Council (to H.Y. and Z.Y.).

#### Ethics statement

The animal experiments were approved by the Veterinary Office of Canton Bern, Switzerland.

#### Conflict of interest

The authors declare no competing interests.

#### Publisher's note

Springer Nature remains neutral with regard to jurisdictional claims in published maps and institutional affiliations.

**Supplementary information** The online version contains supplementary material available at <https://doi.org/10.1038/s41419-021-03668-x>.

Received: 13 March 2020 Revised: 22 March 2021 Accepted: 22 March 2021

Published online: 15 April 2021

#### References

1. Scherpereel, A., Wallyn, F., Albelda, S. M. & Munck, C. Novel therapies for malignant pleural mesothelioma. *Lancet Oncol.* **19**, e161–e172 (2018).
2. Hmeljak, J. et al. Integrative molecular characterization of malignant pleural mesothelioma. *Cancer Discov.* **8**, 1548–1565 (2018).
3. Wu, L. et al. Progress of malignant mesothelioma research in basic science: a review of the 14th international conference of the international mesothelioma interest group (iMiG2018). *Lung Cancer* **127**, 138–145 (2019).
4. Rossini, M. et al. New perspectives on diagnosis and therapy of malignant pleural mesothelioma. *Front. Oncol.* **8**, 91 (2018).
5. Guo, G. et al. Whole-exome sequencing reveals frequent genetic alterations in BAP1, NF2, CDKN2A, and CUL1 in malignant pleural mesothelioma. *Cancer Res.* **75**, 264–269 (2015).
6. Bueno, R. et al. Comprehensive genomic analysis of malignant pleural mesothelioma identifies recurrent mutations, gene fusions and splicing alterations. *Nat. Genet.* **48**, 407–416 (2016).

7. Vogelzang, N. J. et al. Phase III study of pemetrexed in combination with cisplatin versus cisplatin alone in patients with malignant pleural mesothelioma. *J. Clin. Oncol.* **21**, 2636–2644 (2003).
8. Li, W., Cooper, J., Karajannis, M. A. & Giancotti, F. G. Merlin: a tumour suppressor with functions at the cell cortex and in the nucleus. *EMBO Rep.* **13**, 204–215 (2012).
9. Yu, F.-X., Zhao, B. & Guan, K.-L. Hippo pathway in organ size control, tissue homeostasis, and cancer. *Cell* **163**, 811–828 (2015).
10. Benhamouche, S. et al. Nf2/Merlin controls progenitor homeostasis and tumorigenesis in the liver. *Genes Dev.* **24**, 1718–1730 (2010).
11. Hanahan, D. & Weinberg, R. A. Hallmarks of cancer: the next generation. *Cell* **144**, 646–674 (2011).
12. Merino, D. et al. BH3-mimetic drugs: blazing the trail for new cancer medicines. *Cancer Cell* **34**, 879–891 (2018).
13. Fesik, S. W. Promoting apoptosis as a strategy for cancer drug discovery. *Nat. Rev. Cancer* **5**, 876–885 (2005).
14. Leverson, J. D. et al. Exploiting selective BCL-2 family inhibitors to dissect cell survival dependencies and define improved strategies for cancer therapy. *Sci. Transl. Med.* **7**, 279ra240 (2015).
15. Stilgenbauer, S. et al. Venetoclax in relapsed or refractory chronic lymphocytic leukaemia with 17p deletion: a multicentre, open-label, phase 2 study. *Lancet Oncol.* **17**, 768–778 (2016).
16. Broaddus, V. C., Yang, L., Scavo, L. M., Ernst, J. D. & Boylan, A. M. Asbestos induces apoptosis of human and rabbit pleural mesothelial cells via reactive oxygen species. *J. Clin. Invest.* **98**, 2050–2059 (1996).
17. Soini, Y. et al. Apoptosis and expression of apoptosis regulating proteins bcl-2, mcl-1, bcl-X, and bax in malignant mesothelioma. *Clin. Cancer Res.* **5**, 3508–3515 (1999).
18. Xu, D. et al. Increased sensitivity to apoptosis upon endoplasmic reticulum stress-induced activation of the unfolded protein response in chemotherapy-resistant malignant pleural mesothelioma. *Br. J. Cancer* **119**, 65–75 (2018).
19. Jacobson, B. A. et al. Activated 4E-BP1 represses tumorigenesis and IGF-I-mediated activation of the eIF4F complex in mesothelioma. *Br. J. Cancer* **101**, 424–431 (2009).
20. Xu, D. et al. Endoplasmic reticulum stress signaling as a therapeutic target in malignant pleural mesothelioma. *Cancers* **11**, 1502 (2019).
21. Chou, T. C. Drug combination studies and their synergy quantification using the Chou-Talay method. *Cancer Res.* **70**, 440–446 (2010).
22. Xu, D. et al. CRISPR screening identifies WEE1 as a combination target for standard chemotherapy in malignant pleural mesothelioma. *Mol. Cancer Ther.* **19**, 661–672 (2020).
23. Schneider, C. A., Rasband, W. S. & Eliceiri, K. W. NIH image to Image: 25 years of image analysis. *Nat. Methods* **9**, 671–675 (2012).
24. Schlaflí, A. M., Berezowska, S., Adams, O., Langer, R. & Tschan, M. P. Reliable LC3 and p62 autophagy marker detection in formalin fixed paraffin embedded human tissue by immunohistochemistry. *Eur. J. Histochem.* **59**, 2481 (2015).
25. Bankhead, P. et al. QuPath: open source software for digital pathology image analysis. *Sci. Rep.* **7**, 16878 (2017).
26. Parejo, S. et al. Assessing autophagy during retinoid treatment of breast cancer cells. *Methods Mol. Biol.* **2019**, 237–256 (2019).
27. Kinsey, C. G. et al. Protective autophagy elicited by RAF->MEK->ERK inhibition suggests a treatment strategy for RAS-driven cancers. *Nat. Med.* **25**, 620–627 (2019).
28. Yang, H. et al. HSP90/AXL/eIF4E-regulated unfolded protein response as an acquired vulnerability in drug-resistant KRAS-mutant lung cancer. *Oncogenesis* **8**, 45 (2019).
29. Li, J. et al. TCPA: a resource for cancer functional proteomics data. *Nat. Methods* **10**, 1046–1047 (2013).
30. Cerami, E. et al. The cBio cancer genomics portal: an open platform for exploring multidimensional cancer genomics data. *Cancer Discov.* **2**, 401–404 (2012).
31. Tsherniak, A. et al. Defining a cancer dependency map. *Cell* **170**, 564–576 (2017). e516.
32. Barrett, T. et al. NCBI GEO: archive for functional genomics data sets—update. *Nucleic Acids Res.* **41**, D991–D995 (2012).
33. Yang, W. et al. Genomics of drug sensitivity in cancer (GDSC): a resource for therapeutic biomarker discovery in cancer cells. *Nucleic Acids Res.* **41**, D955–D961 (2013).
34. Tate, J. G. et al. COSMIC: the catalogue of somatic mutations in cancer. *Nucleic Acids Res.* **47**, D941–D947 (2019).
35. Juin, P., Geneste, O., Gautier, F., Depil, S. & Campone, M. Decoding and unlocking the BCL-2 dependency of cancer cells. *Nat. Rev. Cancer* **13**, 455–465 (2013).
36. Montero, J. & Letai, A. Why do BCL-2 inhibitors work and where should we use them in the clinic? *Cell Death Differ.* **25**, 56–64 (2018).
37. Certo, M. et al. Mitochondria primed by death signals determine cellular addiction to antiapoptotic BCL-2 family members. *Cancer Cell* **9**, 351–365 (2006).
38. Klionsky, D. J. et al. Guidelines for the use and interpretation of assays for monitoring autophagy (3rd edition). *Autophagy* **12**, 1–222 (2016).
39. Galluzzi, L. et al. Autophagy in malignant transformation and cancer progression. *EMBO J.* **34**, 856–880 (2015).
40. Liu, J. L. et al. Prognostic significance of p62/SQSTM1 subcellular localization and LC3B in oral squamous cell carcinoma. *Br. J. Cancer* **111**, 944–954 (2014).
41. Follo, C., Barbone, D., Richards, W. G., Bueno, R. & Broaddus, V. C. Autophagy initiation correlates with the autophagic flux in 3D models of mesothelioma and with patient outcome. *Autophagy* **12**, 1180–1194 (2016).
42. Zhang, L., Ming, L. & Yu, J. BH3 mimetics to improve cancer therapy: mechanisms and examples. *Drug Resist. Updat.* **10**, 207–217 (2007).
43. Fennell, D. A. & Rudd, R. M. Defective core-apoptosis signalling in diffuse malignant pleural mesothelioma: opportunities for effective drug development. *Lancet Oncol.* **5**, 354–362 (2004).
44. Mohiuddin, I., Cao, X., Fang, B., Nishizaki, M. & Smythe, W. R. Significant augmentation of pro-apoptotic gene therapy by pharmacologic bcl-xL downregulation in mesothelioma. *Cancer Gene Ther.* **8**, 547–554 (2001).
45. Barbone, D. et al. The Bcl-2 repertoire of mesothelioma spheroids underlies acquired apoptotic multicellular resistance. *Cell Death Dis.* **2**, e174 (2011).
46. Cao, X. et al. The novel BH3 alpha-helix mimetic JY-1-106 induces apoptosis in a subset of cancer cells (lung cancer, colon cancer and mesothelioma) by disrupting Bcl-xL and Mcl-1 protein-protein interactions with Bak. *Mol. Cancer* **12**, 42 (2013).
47. Faber, A. C. et al. mTOR inhibition specifically sensitizes colorectal cancers with KRAS or BRAF mutations to BCL-2/BCL-XL inhibition by suppressing MCL-1. *Cancer Discov.* **4**, 42–52 (2014).
48. Opferman, J. T. Attacking cancer's Achilles heel: antagonism of anti-apoptotic BCL-2 family members. *FEBS J.* **283**, 2661–2675 (2016).
49. Budhraja, A. et al. Modulation of navitoclax sensitivity by dihydroartemisinin-mediated MCL-1 repression in BCR-ABL(+) B-lineage acute lymphoblastic leukemia. *Clin. Cancer Res.* **23**, 7558–7568 (2017).
50. Hopkins-Donaldson, S. et al. Induction of apoptosis and chemosensitization of mesothelioma cells by Bcl-2 and Bcl-xL antisense treatment. *Int. J. Cancer* **106**, 160–166 (2003).
51. Jackson, M. R. et al. Mesothelioma cells depend on the antiapoptotic protein Bcl-xL for survival and are sensitized to ionizing radiation by BH3-mimetics. *Int. J. Radiat. Oncol. Biol. Phys.* **106**, 867–877 (2020).
52. Galluzzi, L. et al. Molecular mechanisms of cell death: recommendations of the Nomenclature Committee on Cell Death 2018. *Cell Death Differ.* **25**, 486–541 (2018).
53. Maiuri, M. C., Zalckvar, E., Kimchi, A. & Kroemer, G. Self-eating and self-killing: crosstalk between autophagy and apoptosis. *Nat. Rev. Mol. Cell Biol.* **8**, 741–752 (2007).
54. Marino, G., Niso-Santano, M., Baehrecke, E. H. & Kroemer, G. Self-consumption: the interplay of autophagy and apoptosis. *Nat. Rev. Mol. Cell Biol.* **15**, 81–94 (2014).
55. Fitzwalter, B. E. et al. Autophagy inhibition mediates apoptosis sensitization in cancer therapy by relieving FOXO3a turnover. *Dev. Cell* **44**, 555–565 (2018). e3.
56. Gump, J. M. & Thorburn, A. Autophagy and apoptosis: what is the connection? *Trends Cell Biol.* **21**, 387–392 (2011).
57. Pedro, J. M. et al. BAX and BAK1 are dispensable for ABT-737-induced dissociation of the BCL2-BECN1 complex and autophagy. *Autophagy* **11**, 452–459 (2015).
58. Reljic, B. et al. BAX-BAK1-independent LC3B lipidation by BH3 mimetics is unrelated to BH3 mimetic activity and has only minimal effects on autophagic flux. *Autophagy* **12**, 1083–1093 (2016).
59. Lin, Q. H. et al. ABT-263 induces G1/G0-phase arrest, apoptosis and autophagy in human esophageal cancer cells in vitro. *Acta Pharm. Sin.* **38**, 1632–1641 (2017).
60. Arulananda, S. et al. BCL-XL is an actionable target for treatment of malignant pleural mesothelioma. *Cell Death Discov.* **6**, 114 (2020).